energies

MDPI

Article

Numerical Simulation of Subcooled Flow Boiling in a Threaded Tube and Investigation of Heat Transfer and Bubble Behavior

Ke Lei [1,2], Jinfeng Wang [1,2,3,4,*], Jing Xie [1,2,3,4,*] and Bingjun Wang [1,2]

[1] College of Food Science and Technology, Shanghai Ocean University, Shanghai 201306, China; 2036223@st.shou.edu.cn (K.L.); m200300788@st.shou.edu.cn (B.W.)
[2] Shanghai Professional Technology Service Platform on Cold Chain Equipment Performance and Energy Saving Evaluation, Shanghai 201306, China
[3] National Experimental Teaching Demonstration Center for Food Science and Engineering, Shanghai Ocean University, Shanghai 201306, China
[4] Quality Supervision, Inspection and Testing Center for Cold Storage and Refrigeration Equipment, Ministry of Agriculture, Shanghai 201306, China
* Correspondence: jfwang@shou.edu.cn (J.W.); jxie@shou.edu.cn (J.X.); Tel.: +86-15692165513 (J.X.)

Abstract: Three-dimensional subcooled flow boiling of R134a in a threaded tube was numerically simulated at the conditions of 200~400 kW/m^2 heat flux, 3~20 K inlet subcooling, and 0.2~0.6 m/s inlet velocity. The bubble behavior in the horizontal threaded tube with 0.581 mm thread tooth height was observed. The effect of heat flux, inlet subcooling, and inlet velocity on bubble departure diameter and heat transfer coefficient were explored. The results presented the whole growth process of five kinds of bubbles. It was found that the bubbles either collapsed in cold liquid after leaving the heating wall or grew along the axial direction and contacted the heating wall. And there was no bubble sliding during the growth. In addition, the most important and special characteristic of bubble behavior in threaded tubes was the phenomenon of the bubble passing through the cavity. The coalescence and breakup behavior occurred after the bubble passed through the cavity. According to the discussions of the departure diameter and heat transfer coefficient, it was inferred that the bubble departure diameter increased with the increase of heat flux from 200~400 kW/m^2 and subcooling from 3~20 K while decreasing with the increase of inlet velocity from 0.2~0.6 m/s. And due to the influence of the threaded tube structure, there are special points in the change of bubble departure diameter. The heat transfer coefficient of the bubbles in the threaded tube was higher than the smooth tube, which was increased by 1.5~12.5%. The heat transfer coefficient increased with the increase of heat flux and subcooling and is closely related to the bubble departure diameter.

Keywords: threaded tube; subcooled flow boiling; bubble behavior; bubble departure; heat transfer coefficient

Citation: Lei, K.; Wang, J.; Xie, J.; Wang, B. Numerical Simulation of Subcooled Flow Boiling in a Threaded Tube and Investigation of Heat Transfer and Bubble Behavior. *Energies* **2023**, *16*, 5719. https://doi.org/10.3390/en16155719

Academic Editors: Dmitry Eskin and Gianpiero Colangelo

Received: 21 May 2023
Revised: 21 June 2023
Accepted: 27 July 2023
Published: 31 July 2023

1. Introduction

In the field of heat transfer, more and more small-diameter enhanced tubes are used in small refrigeration systems., mainly threaded tubes. Compared with a smooth tube, the threaded tube not only increases the heat transfer area but also enhances the fluid disturbance so that the heat transfer is augmented. Celen et al. [1] conducted research on the heat transfer characteristics of R134a in micro-fin tubes. The conclusion was that the boiling heat transfer coefficient of the micro-finned tube with an 8.63 mm inner diameter was 1.9 times higher than the smooth tube. Yang and Hrnjak [2] utilized a 3D technique to print threaded tubes with a 6.327 mm inner diameter and explored the influence of micro-fin geometries on flow patterns. Yarmohammadi et al. optimized the 8.7 mm inner diameter corrugated tube evaporator with R404A as the working fluid, and the heat transfer coefficient is 33% higher than that of the smooth tube [3]. He et al. [4] investigated the flowing boiling heat transfer characteristics of R32 in micro-fin tubes and found that

compared with a smooth tube, the enhancement coefficients of the 5 mm micro-fin tube is about 1.19 times and that of the 7 mm micro-fin tube is about 1.23 times. However, the above research mostly adopted large-diameter threaded tubes, and the investigations of small-diameter threaded tubes are not sufficient. Considering that the small-diameter threaded tubes can greatly reduce the cost of the heat exchanger and refrigerant charge [5], the heat transfer characteristics of small-diameter threaded tubes are worth exploring, especially the 3~5 mm tube diameter.

Different from the heat transfer of a single phase, the heat transfer efficiency of boiling is greatly improved by the phase transition process [6,7]. An important way of boiling heat transfer in a tube is subcooled flow boiling. Subcooled flow boiling refers to the phenomenon of flow and phase change under heated conditions, which includes a complex combination of turbulence, multiphase flow, and phase-change heat transfer. Subcooled flow boiling refers to the boiling heat transfer when the main temperature of the liquid is lower than the saturation temperature under the corresponding pressure and the wall temperature is greater than the saturation temperature. The bubbles generated from the heating wall have not departed, or have been condensed and disappeared in the bulk liquid after departing, so the boiling can only be limited to a thin layer of superheated liquid close to the heating surface. At this time, due to the continuous generation and condensation of bubbles, the liquid is greatly disturbed, so the heat transfer is significantly enhanced. At the same time, subcooled flow boiling can reduce the occurrence of wall evaporation to dryness. Bubble generation requires a mass of latent heat and transports energy from a hot region to a cold liquid in subcooled flow boiling [8]. Subcooled flow boiling is applied to many fields, such as pulsating heat pipes, refrigeration, nuclear, electronic cooling, biological engineering, and aerospace [9–12].

Bubble behavior and dynamics are the keys to heat transfer enhancement in tubes [13,14]. Under the condition of subcooled flow boiling, the existence of bubbles will significantly affect the heat transfer environment and flow stability of the system. More and more attention has been paid to bubble behavior in subcooled flow boiling because a better understanding and prediction of bubbles are critical for heat transfer mechanisms and enhancement in subcooled flow boiling [15,16]. Yu et al. [17] investigated sliding bubble dynamics in vertical subcooled flow boiling. It was concluded that the growth of sliding bubbles is greatly affected by the condensation of subcooled liquid bulk and the diameter follows a lognormal distribution due to the bubble coalescence, while the sliding velocity distribution is not affected by the thermal condition and conforms to a normal distribution. Yang et al. [18] studied upward subcooled flow boiling in a narrow channel through experiments. The results showed that the onset of nucleate boiling relied strongly on wall superheat and heat flux. The mass flux, wall superheat, and subcooling had a considerable impact on bubble departure diameter. At present, a high-speed camera is used to realize visualization for the investigations of bubble behavior [19–21]. However, a high-speed camera is expensive and the flow details in the tube cannot be expressed enough. CFD (computational fluid dynamics) is a powerful tool for process optimization and quantitative design [22,23]. And the flow details in a tube, for example, bubble behavior, can be detailed clearly by CFD. In recent years, research on subcooled flow boiling through numerical simulation has become popular [24–26].

The phase-interface behavior has a great influence on the characteristics of two-phase flow heat and mass transfer. The VOF (volume of fluid) model and the level-set method are two different research methods for tracking phase-interface behavior. Zhuan and Wang [27] used the VOF model to simulate the subcooled flow boiling, which observed bubble behavior and analyzed the mechanism of subcooled boiling in channels. Kang et al. used the VOF model to study the effect of a porous wicking layer on the heat transfer characteristics of a single-loop pulsating heat pipe [28]. Lee et al. [29] used the level-set method to explore the process of bubble growth and boiling heat transfer on micro-fins. The experiment discovered that micro-fins can enhance boiling heat transfer and determined the optimal structure of micro-fins by tracking bubbles. The VOF model was also adopted

to develop a new pulsating heat pipe [30]. At present, there are few studies on subcooled flow boiling with the combination of the VOF model and the level-set method. In addition, the refrigerant subcooled flow boiling in the threaded tube is more complicated, so it is necessary to adopt the VOF model and the level-set method for bubble capture in subcooled flow boiling in threaded tube.

Based on the above discussion, the study of refrigerant R134a subcooled boiling is of great significance for improving the performance of refrigeration systems. The purpose of this study is to explore the subcooled boiling heat transfer characteristics and bubble behavior of refrigerant R134a in small-diameter threaded tubes under different working conditions. The bubble behavior characteristics of R134a in subcooled boiling of small-diameter threaded tubes under the conditions of mass flow rate of 0.2~0.6 m/s, subcooling of 3~20 K, and heat flux of 200~400 kW/m^2 are numerically simulated in this paper. The VOF model coupled with the level-set method is used to track the gas-liquid interface, and the characteristics of bubble behavior, bubble departure diameter, and heat transfer coefficient are explored and analyzed.

2. Numerical Methods

2.1. Mesh in ICEM

The software ICEM 2020 R2 was used to establish a three-dimensional geometric model of the threaded tube and meshed the geometric model. Figure 1 shows the sketch of the geometric model. The working fluid R134a flowed and boiled in the 3.715 mm gap formed by tubes with an inner diameter of 8.57 mm, an outer diameter of 16 mm, and a length of 100 mm. The front 10 mm and the end 10 mm of the inner tube were smooth, and the other positions were set by standard threads. The simulation used a 55° sealed tube thread with a thread tooth height of 0.581 mm and a pitch of 0.907 mm. In order to improve the precision of the VOF model, the O-block mesh was adopted for the geometric model of the threaded tube shown in Figure 2a. The mesh of the heating wall generated by ICEM is depicted in Figure 2b. The mesh on the heating surface was refined when meshing, considering the minimum departure diameter of the R134a bubble was about 0.1 mm, and the first layer of mesh was set to 0.11 mm. Through an analysis of the simulation results, the number of grids was adjusted repeatedly. Finally, the generated number of grids in the gap was 6638208.

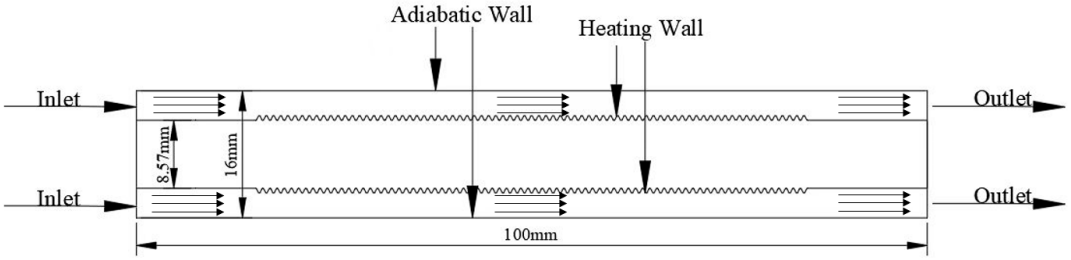

Figure 1. The sketch of the geometric model.

2.2. Governing Models and Equations

In this simulation of subcooled flow boiling on a heating wall with a thread, some subcooled flow boiling models were selected, including the multiphase VOF model, the level-set method, the SST k-ω model, and the phase change model. The multiphase VOF model and the level-set method were used to determine the two-phase interface. The VOF model can accurately construct the phase interface, which requires a short calculation time and less storage. The level-set model has a strong ability to handle complex interfaces. The shear stress effect caused by turbulence near the wall during subcooled boiling around the bubble was considered by the SST k-ω model [31]. The phase change model acts in a mesh cell to determine the conditions of two-phase heat and mass transfer. The above

models consist of multivariable equations, which are solved by determining the material and boundary conditions in Fluent solver.

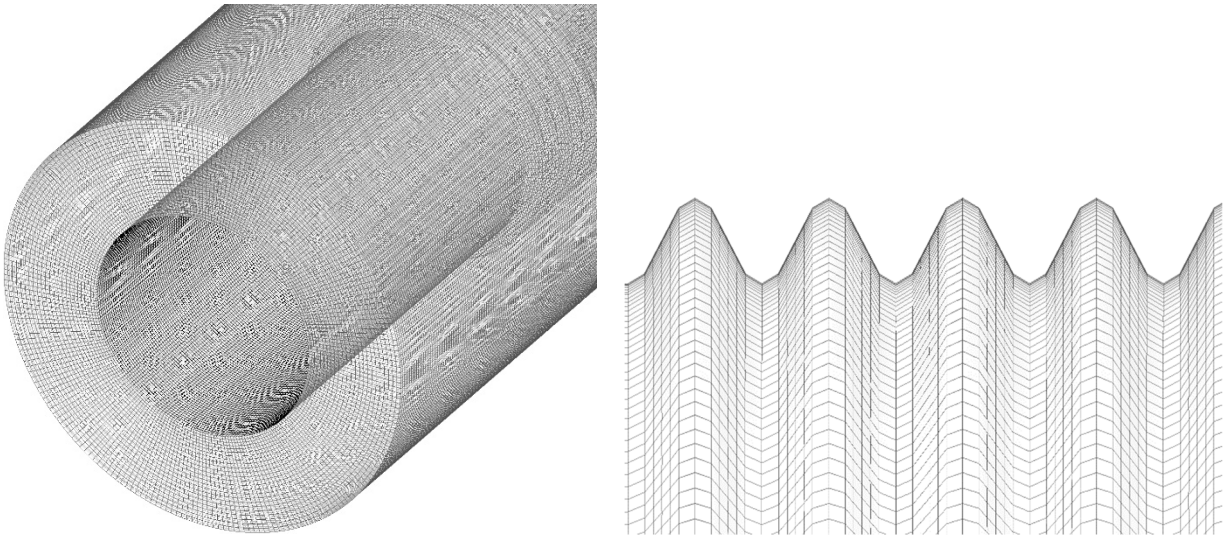

(**a**) (**b**)

Figure 2. The mesh generated by ICEM (**a**) and the mesh of the heating wall generated by ICEM (**b**).

The main equations to be solved by the Fluent solver include the continuity equation, momentum equation, energy equation, turbulent k-ω equation, and phase change equation. The specific mathematical form is as follows.

The continuity equations with the VOF model:

$$\frac{\partial \alpha_v}{\partial t} + \nabla \cdot (\vec{u}\alpha_v) = \frac{M_{lv}}{\rho_v} \tag{1}$$

$$\frac{\partial \alpha_l}{\partial t} + \nabla \cdot (\vec{u}\alpha_l) = \frac{M_{vl}}{\rho_l} \tag{2}$$

$$\alpha_l + \alpha_v = 1 \tag{3}$$

where ρ and u stand for the fluid density and velocity, subscript l and v are the liquid and vapor phase, M_{lv} is the mass source from the liquid phase to the vapor phase, M_{vl} is the mass source from the vapor phase to the liquid phase, and α represents the volume fraction and controls the phase where $\alpha = 0$ is for vapor phase, $\alpha = 1$ is for the liquid phase and $0 < \alpha < 1$ is for the liquid–vapor interface.

The momentum equation is shared by two phases with the VOF model:

$$\frac{\partial \rho \vec{u}}{\partial t} + \nabla \cdot (\rho \vec{u}\vec{u}) = -\nabla p + \nabla \cdot [\mu_{eff}(\nabla \vec{u} + \nabla \vec{u}^T)] + \rho \vec{g} + \vec{F}_{vol} \tag{4}$$

where p stands for the fluid domain pressure, μ_{eff} stands for the effective dynamic viscosity, $\vec{u}^T$ stands for the transpose part of the strain rate tensor, g stands for the acceleration of gravity, and $\vec{F}_{vol}$ stands for the surface tension per unit volume of fluid.

The fluid momentum equation combined with the level-set method is,

$$\frac{\rho(\phi)\partial \vec{u}}{\partial t} + \rho(\phi)\nabla \cdot (\vec{u}\vec{u}) = -\nabla p + \mu(\phi)\nabla \cdot [(\nabla \vec{u} + \nabla \vec{u}^T)] + \rho(\phi)\vec{g} + \vec{F}_{level} \tag{5}$$

where $\rho(\phi)$ and $\mu(\phi)$ stand for density smoothed and viscosity smoothed. ϕ stands for a signed distance from the interface.

The energy equation is shared by two phases with the VOF model:

$$\frac{\partial \rho c_p T}{\partial t} + \nabla(\vec{u}(\rho c_p T + p)) = \nabla(\lambda_{eff} \nabla T) + S_E \tag{6}$$

where T stands for the temperature, c_p stands for the mixture-specific heat capacity, λ_{eff} is the effective thermal conductivity, and S_E is the energy source term that is loaded by the UDF (user-defined function).

The turbulence equations with the SST k − ω model:

$$\frac{\partial \rho k}{\partial t} + \nabla \cdot (\rho k \vec{u}) = \nabla \cdot [(\nu + \frac{\nu_t}{\sigma_k}) \nabla \cdot k] + G_k - Y_k \tag{7}$$

$$\frac{\partial \rho \omega}{\partial t} + \nabla \cdot (\rho \omega \vec{u}) = \nabla \cdot [(\nu + \frac{\nu_t}{\sigma_\omega}) \nabla \cdot \omega] + G_\omega - Y_\omega + D_\omega \tag{8}$$

Equations (7) and (8) are for solving k and ω. k and ω stand for the turbulent kinetic energy and turbulent vortex frequency, and ν_t stands for turbulent kinematic viscosity. σ_ω is the reciprocal of the effective turbulent Prandtl number of the turbulent vortex frequency, σ_k is the reciprocal of the effective turbulent Prandtl number of turbulent kinetic energy, G_k is the generation term of turbulent kinetic energy caused by time-average velocity gradient, G_ω is the generation term of turbulent vortex frequency, Y_k is the dissipation term of turbulent kinetic energy, Y_ω is the dissipation term of turbulent vortex frequency, and D_ω is the cross-diffusion term.

The Lee model is a dynamic model that is driven by temperature difference and has obvious physical sense. The bubbles' motion can be expressed more clearly by the Lee model. At the same time, UDF is imported into the Fluent solver to redevelop the Lee model, so as to construct R134a bubbles more accurately. More details can be found in the author's previous work [32]. The Lee model [33] is selected as the phase change model in Equations (9)–(11):

$$M_{lv} = -\eta \alpha_l \rho_l \frac{T - T_{sat}}{T_{sat}} (if\ T > T_{sat}) \tag{9}$$

$$M_{vl} = \eta \alpha_v \rho_v \frac{T_{sat} - T}{T_{sat}}\ (if\ T < T_{sat}) \tag{10}$$

$$S_E = hM \tag{11}$$

where η stands for the phase change mass transfer coefficient, T_{sat} stands for saturation temperature and h stands for latent heat. In the simulation, the saturation temperature was 288.15 K, and η was 10.

2.3. Simulation Settings

In the simulation, the physical properties of materials obtained by REFPROP 9.1 software are shown in Table 1. Considering the sensitivity of specific heat capacity with temperature in the process of subcooled flow, the specific heat capacity is input in a piecewise-linear manner as shown in Figure 3. In addition, the wall contact angle was 17°. The type and the specific values of boundary conditions were determined according to the research purpose. In this paper, the bubble behavior and heat transfer in the threaded tube under different heat fluxes, inlet velocities, and inlet subcooling conditions were studied. Therefore, certain boundary conditions were set, as shown in Table 2. Based on the boundary conditions and the physical properties of materials, variables at different times can be solved by an explicit scheme. An explicit scheme was used to solve time-dependent dynamic problems in Fluent solver. Its advantage is that the simultaneous solution of the equation is reduced and the calculation workload is small. In addition, the discretization and solution of control equations were completed by algorithm setting. The algorithms include PISO for pressure-velocity couple and Green–Gauss node based for

spatial discretization. The PISO [34] was used for the solution of velocity and the Green-Gauss node was used for the gradient solution. The above algorithm had the advantages of stability, advancement, and accuracy. The second-order upwind scheme was used to ensure the accuracy of momentum and energy equations. The geo-reconstruction method was used for sharp interface morphology to reconstruct the bubble boundary more accurately. Finally, the time step was 0.05 ms.

Table 1. The properties of the working fluid.

Fluid	Density (kg/m^3)	Thermal Conductivity (W/(m·K))	Viscosity (Pa·s)	Surface Tension (N/m)	Temperature (K)	Pressure (MPa)
R134a liquid	1243.4	0.085	2.21×10^{-4}	0.009	288.15	0.48837
R134a vapor	23.758	0.0129	1.13×10^{-5}	-	288.15	0.48837

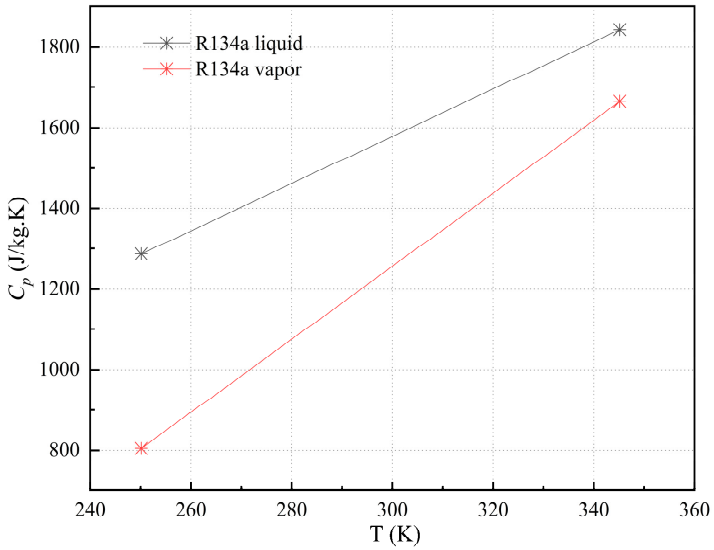

Figure 3. The specific heat capacity in a piecewise-linear manner.

Table 2. More details of the setting.

Position	Type	Content	
Inlet	Mass flow inlet	Mass Flow Rate (kg/s):	0.022, 0.033, 0.044, 0.055, 0.066
		Inlet temperature (K):	285.15, 284.15, 282.15, 278.15, 273.15, 268.15
		Supersonic/Initial Gauge pressure (atm):	4.8199
Outlet	Pressure outlet	Gauge pressure (atm):	4.85
Heating wall	wall	Heat flux (W/m^2):	200,000, 250,000, 300,000, 350,000, 400,000
		Material name:	copper
		wall thickness:	0.5 mm
Adiabatic wall	wall	Heat flux (W/m^2):	0
		Material name:	copper
		wall thickness:	0.5 mm

3. Results and Discussion

3.1. Validation of Simulation

For the above-built subcooled flow boiling model, the validation of the simulation was performed by Chen's [35] experiment data. The heat transfer coefficient was calculated based on Equation (12) and was used as the validation index of the model.

$$h_r = \frac{q}{T_f - T_m} \tag{12}$$

where q stands for the heat flux, T_f stands for the fluid temperature, and T_m stands for the wall temperature.

The working conditions of Chen's experiment are as follows: the mass flow rate is 500 kg/(m^{2}s), the heat flux is 16 kW/m^2~40 kW/m^2, the saturation temperature is 288.15 K, and the subcooling is 3 K. And the working fluid is R134a. According to Chen et al.'s [35] experiment, the selected simulation conditions are at different heat fluxes, 3 K subcooling, and 0.4 m/s velocity. A detailed comparison of the heat transfer coefficient between the simulation and experiment was shown in Figure 4. The relative error of the heat transfer coefficient is in the range of 2.68% and 5.4% for the different heat fluxes. On the one hand, there will be errors in the setting of inlet velocity and wall heat flow during the experiment. On the other hand, relative errors occurred due to the selection of models and computer processors. In addition, the heat transfer coefficient of experimental and simulated models increased with heat flux from 15~40 kW/m^2. It can be inferred that the simulation and experimental models have achieved good consistency. Therefore, the model constructed in this paper is effective.

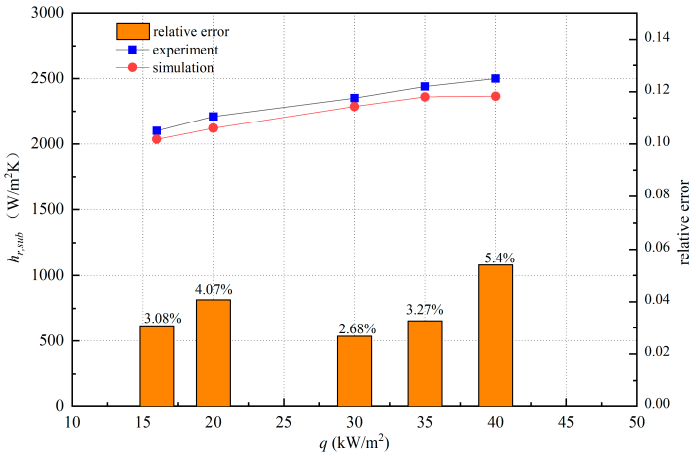

Figure 4. A detailed comparison of heat transfer coefficient between simulation and experimental models.

According to the characteristics of flow boiling, the bubble departs from the boundary layer that belongs to the buffer layer. The buffer layer region is the region where viscosity and Reynold stress are obvious. Therefore, the first layer cell uses $7 < y^+ < 14$ to ensure that the near-wall region is within the buffer region [36]. The equation of y^+ is,

$$y^+ = \frac{yu_\tau}{v} \tag{13}$$

where y stands for the boundary layer length, u_τ stands for the shear velocity, and v stands for the kinematic viscosity.

During the simulation, the value of y^+ was monitored as shown in Figure 5. The value of y^+ is in the range of 7~14, which meets the requirements of the turbulence model, and tends to be stable with the extension of simulation time. It proves that the method used and the number of grids are appropriate.

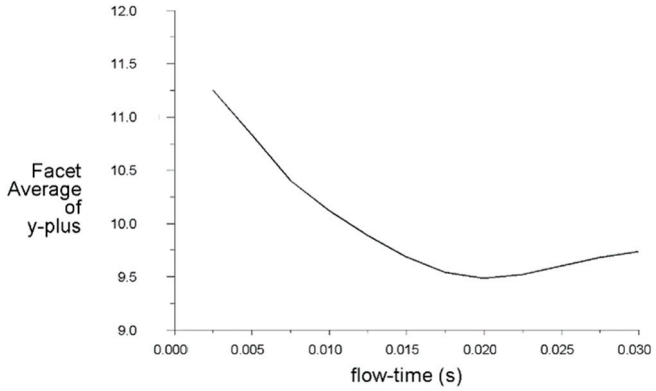

Figure 5. The value of y^+ monitored during the simulation.

3.2. Bubble Behavior

Bubble behavior during subcooled boiling in the threaded tube is observed clearly at conditions of 300 kW/m^2 heat flux, 0.4 m/s inlet velocity, and 4 K subcooling. The process of bubble nucleation in the threaded tube is shown in Figure 6, which shows there is a bubble nucleation in each cavity. The reason behind this is that the liquid in the cavity is strongly heated. The simulation further confirms that bubble nucleation forms easier in the cavity. Furthermore, it is inferred that the increase of the cavity provides the possibility to further enhance the subcooled boiling heat transfer. However, for a certain tube length, the space of a single cavity will be reduced due to the increasing cavity density, which affects the radial and axial growth of bubbles in the cavity. The smaller bubbles or even the coalescence of bubbles after departure might negatively impact the heat transfer [37].

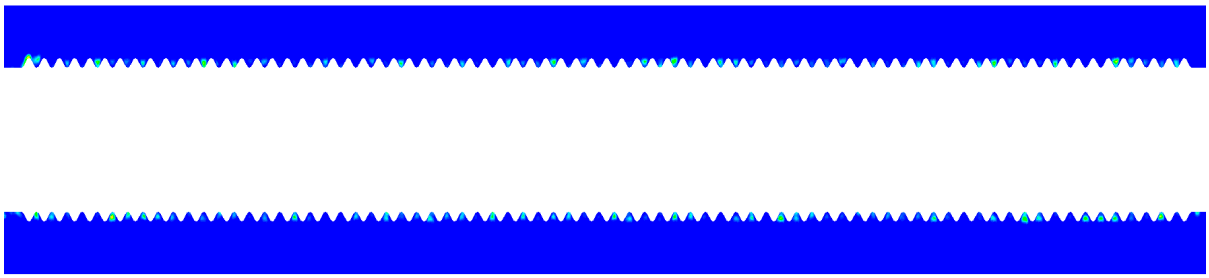

Figure 6. The process of bubble nucleation in the threaded tube.

Figure 7a shows the entire growth of five kinds of bubbles, the bubbles are marked with a red box, and B is the abbreviation of bubble. Bubble B1 shows the process of nucleation, growth, and departure in the cavity. It can be seen from Figure 7a that bubble B1 nucleated at 10 ms and then departed at 12.5 ms. Bubble B2 shows the classical process of bubble growth in subcooled boiling, including bubble nucleation, bubble growth, bubble departure, and collapse. To be more concrete, the process of bubble growth can be described by time. The bubble B2 nucleates under surface tension at 5 ms, grows with increasing size during 5 ms and 11 ms, departs from the heating wall during 11 ms and 12 ms, and collapses in cold liquid. The bubble growth in the cavity shows certain characteristics. Bubble B2 grows along the radial direction, and the growth of bubbles B1, B3, B4, and B5 also have this growth characteristic. Unlike bubble B2, the other bubbles do not collapse after departure but grow in the axial direction. It is explained that there is a special evolution of the temperature field in the cavity as shown in Figure 7b. It can be seen from Figure 7c that the temperature gradient between bubble B2 and the upper main stream cold fluid is greater than that of other bubbles at 10.5 ms. According to the speculation, this shows that bubble B2 is prematurely affected by the temperature of the main stream cold fluid during the growth process, resulting in bubble B2 being condensed by the main stream cold fluid before departure. The temperature field at 6.5 ms and 9 ms provides a growth

environment for the radial generation of bubbles, while the temperature field at 10.5 ms provides an environment for the axial growth of bubbles. Interestingly, bubble growth in the threaded tube is different from that in the smooth tube. There is no bubble sliding during the bubble-growth process, which may be related to the hindrance of the threaded structure. In addition, the bubble contacts the cavity wall due to the axial growth and flow effects of the bubble after departure, such as bubbles B3, B4, and B5. Figure 7d shows the zoomed view of bubbles, which are marked with a black box in Figure 7a. It is observed that the bubble re-contacts the heating wall and then grows again. The continuous growth of the bubble provides conditions for the bubble to communicate across the cavity, which will be discussed below.

As discussed above, bubbles appear to cross the cavity. Figure 8 shows the coalescence and breakup behavior of the bubbles after crossing the cavity. The bubbles generated in the cavity of the threaded tube will occupy the cavity and grow alone. There is no possibility for the coalescence of bubbles during the growth of the cavity. Therefore, the coalescence needs to be carried out across the cavity and requires the growth of bubbles in adjacent cavities. Bubble coalescence is realized after the bubbles in Figure 8a meet the conditions. If the bubbles growing across the cavity do not encounter the bubbles in the adjacent cavity, the breakup behavior occurs, as shown in Figure 8b. The analysis suggests that this may be related to the temperature field and flow disturbance. Both sides of the cavity provide a hot environment, and the upper part of the cavity is cooled by the main stream, so the temperature field is distorted, and the bubble breaks under the action of surface tension. Whether it is bubble coalescence or bubble breakup, the heat transfer of bubbles is enhanced. The possible reason is that the bubble coalescence and breakup disturb the fluid, which aggravates the degree of turbulence and promotes the convective heat transfer between the bubble and the main fluid. Therefore, the way to enhance heat transfer in this study is to promote the exchange of bubbles across the cavity as much as possible.

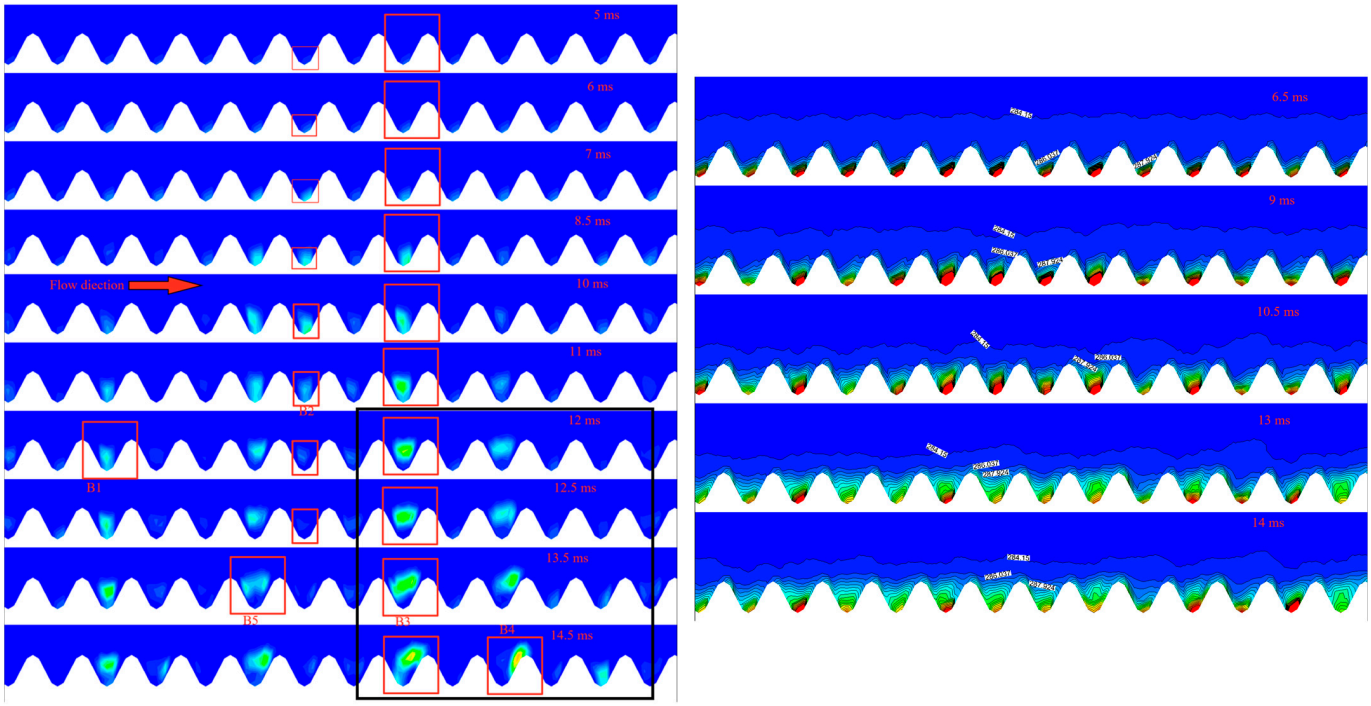

(**a**) (**b**)

Figure 7. *Cont.*

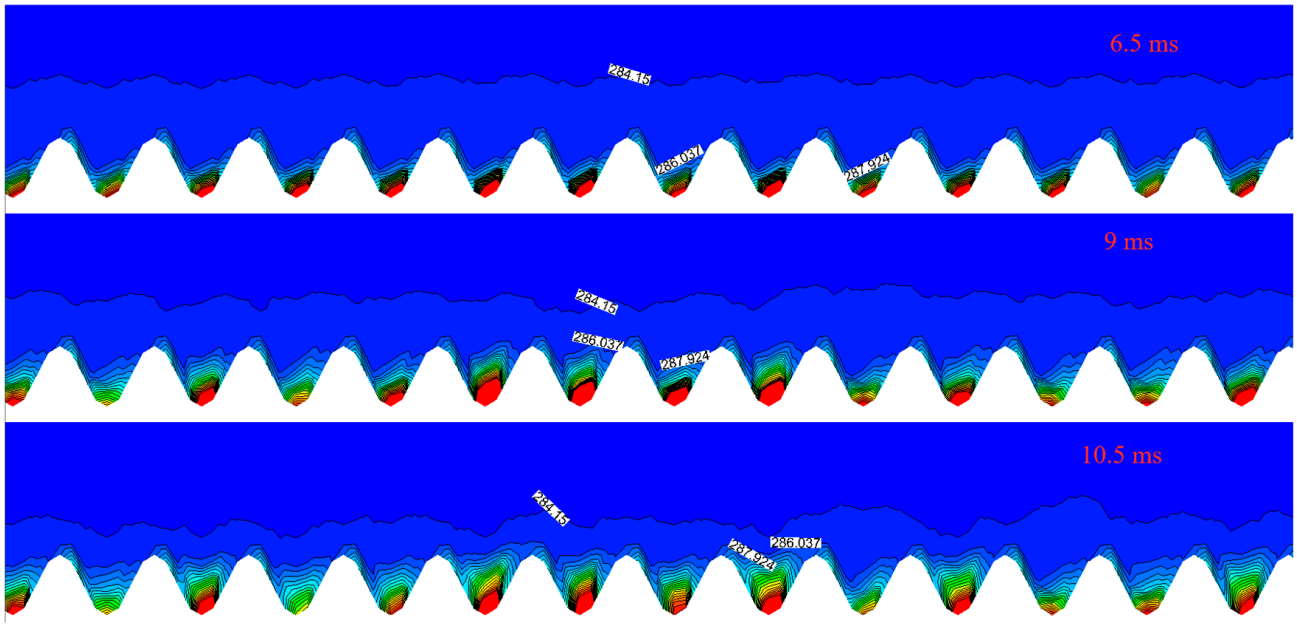

(**c**)

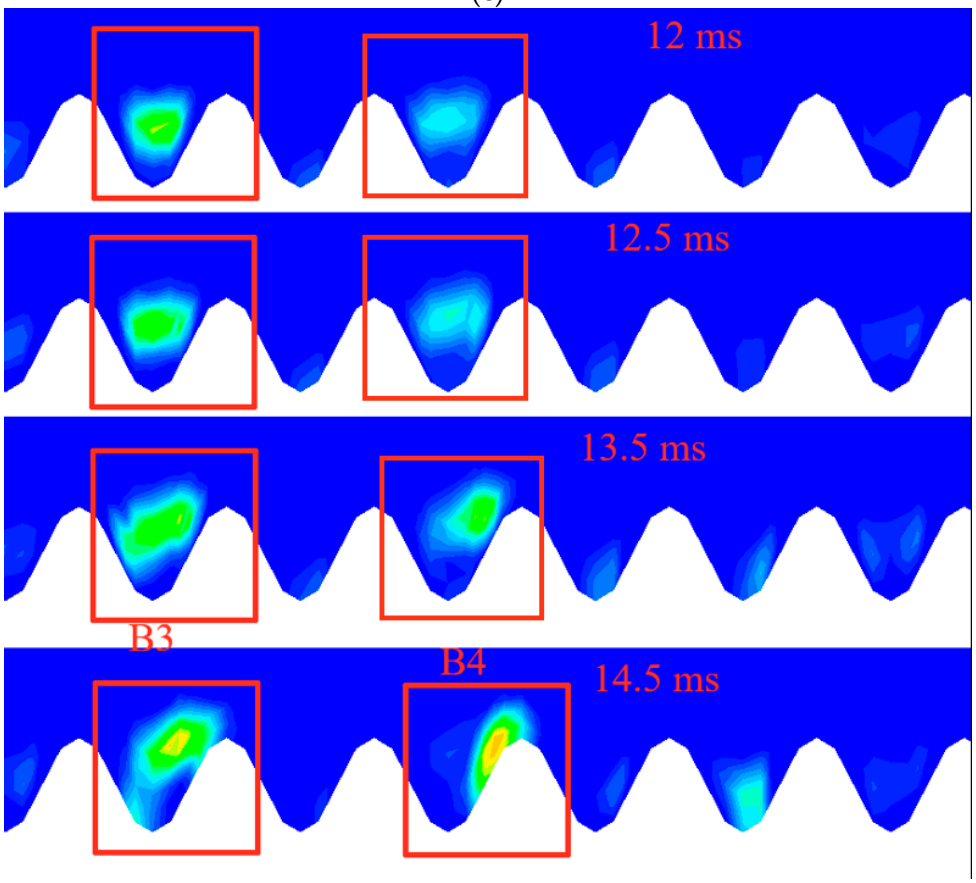

(**d**)

Figure 7. The entire growth of five bubbles (**a**), a special evolution of temperature field in a cavity (**b**), the zoomed view of temperature field (**c**), and the zoomed view of bubbles which are marked with a black box in (**d**).

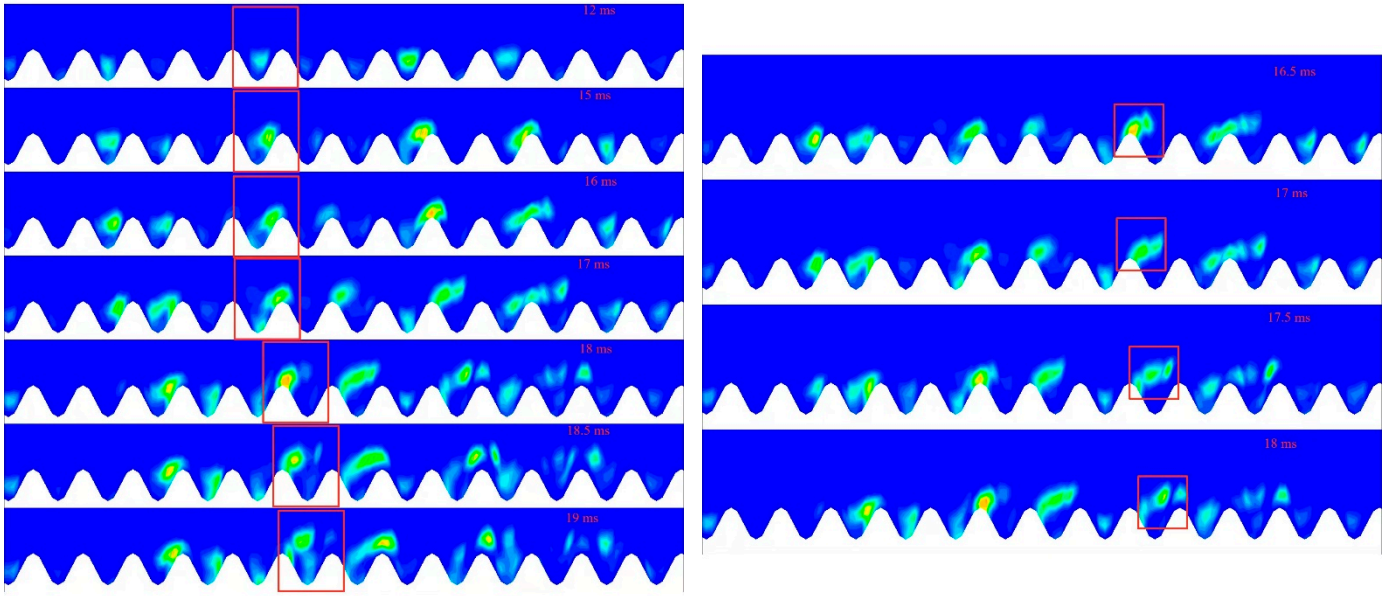

(**a**) (**b**)

Figure 8. Bubbles appear to cross the cavity for the coalescence (**a**) and breakup behavior (**b**).

3.3. Bubble Departure Diameter

The bubble phenomena in subcooled boiling in threaded tubes show that bubbles in the cavity grow radially to a certain size at nucleation sites and then depart from the heating wall. The bubble diameter was introduced to investigate the heat transfer in a threaded tube, which is calculated by Equations (14) and (15) of Han and Griffith [38]. In the previous study of subcooled boiling in smooth tubes, the authors found that bubbles nucleate and slide along the heating surface, grow along the axis and coalesce with other bubbles to form larger bubbles, but most of the bubbles collapse after leaving the wall. According to the investigation, the bubble departure diameter in the threaded tube is between 0.2 mm and 0.3 mm at conditions of 200~400 kW/m^2 heat flux, 0.2~0.6 m/s inlet velocity, and 3~20 K inlet subcooling, while the diameter of bubble departure in the smooth tube can reach between 0.25 mm and 0.35 mm, and even 0.4 mm in the smooth tube at the condition of 200~400 kW/m^2 heat flux, 0.2~0.4 m/s inlet velocity, and 3~10 K inlet subcooling. Obviously, due to the limitation of the thread, the bubbles cannot slide, and the diameter of the bubble departure in the threaded tube is generally smaller than that of the smooth tube, but the threaded tube enables the bubbles to achieve secondary growth and departure, thereby enhancing the heat transfer.

$$D = \sqrt{ab} \tag{14}$$

$$D_{ave} = \frac{1}{n}\sum_{i=1}^{n} D_i \tag{15}$$

In addition, the influence of heat flux, inlet velocity, and inlet subcooling on bubble departure diameter is investigated at the condition of 0.581 mm tooth height. Figures 9–11 present the bubble departure diameters at different heat fluxes, inlet subcooling, and velocities. It is found that the bubble departure diameter increases with the increase of heat flux from 200~400 kW/m^2 and inlet subcooling from 3~20 K while decreasing with the increase of inlet velocity from 0.2~0.6 m/s. The effect of heat flux on bubble departure is manifested in two aspects. On the one hand, the heat flux directly heats the gas in the bubble, which increases the volume of the bubble. On the other hand, the heat flux of the

bubble provides a superheating environment for the bubble, so that the bubble can expand around, and these two advantages are more pronounced under high heat flux conditions. However, in the range of 300~400 kW/m^2 heat flux, the bubble departure diameter does not change much, which may be related to the influence of the thread structure, the bubble reaches a certain size and then departs from the heating wall. When the bubble grows to a larger size, the limitation of the thread is reflected. And the bubble velocity is constant, which may also be one of the reasons why the bubble departure diameter does not change much. But when the heat flux is greater than 350 kW/m^2, the bubble departure diameter decreases. It is speculated that the effect of buoyancy on bubbles is enhanced under high heat flux, promoting the radial departure of bubbles.

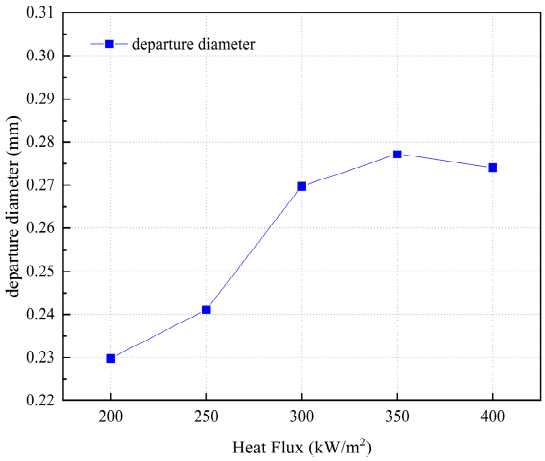

Figure 9. The bubble departure diameters at different heat fluxes.

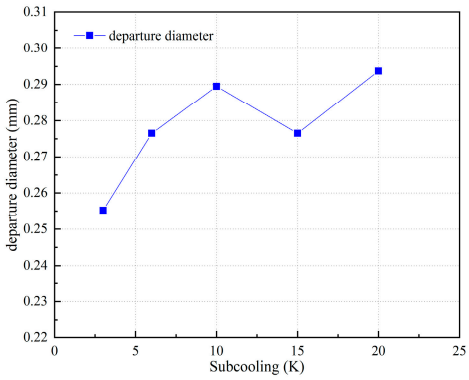

Figure 10. The bubble departure diameters at different inlet subcooling.

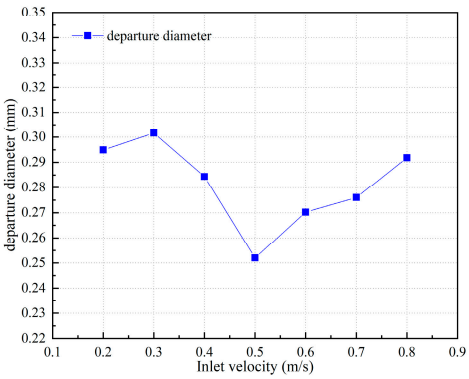

Figure 11. The bubble departure diameters at different velocities.

According to Figure 10, as the inlet subcooling increases, the bubble departure diameter clearly increases. This contributes to the enhancement of the Marangoni effect when

inlet subcooling increases, and adds enough heat flux provided by the heating wall, which results in the augmentation of the bubble departure diameter. Under a certain degree of subcooling, a temperature gradient will be generated and the surface tension dominated by the temperature gradient causes the interface to move to a lower temperature region. It should be noted that the heat provided by the wall is sufficient to increase bubble size, otherwise, the bubble will be pulled away from the wall by the interface. But when the inlet subcooling is 15 K, the bubble departure diameter decreases. It is speculated that the temperature field in the threaded tube has changed greatly due to the effect of the threaded structure at the inlet subcooling of 15 K so that the unstable turbulence in the threaded tube is intensified, which affects the surface tension of the bubble [39].

Figure 11 shows that the bubble departure diameter decreases as inlet velocity increases, which is mainly owed to the suppression of the main stream. The main-stream velocity increases at high inlet velocities, resulting in an unstable bubble-growth environment. And, under the condition of high-inlet velocity, the shear force acting on the bubble increases, thus promoting the departure of the bubble. The main stream has the strongest suppression on bubble growth at the inlet velocity of 0.5 m/s. When the inlet velocity further increases from 0.5 m/s, the bubble departure diameter increases. It is speculated that when the inlet velocity continues to increase, the influence of the main stream on the adjacent thread cavities far from the main stream is decreased, and the protective effect of the thread on bubble growth is greater than the suppression of the main stream in the threaded tube on bubble growth. Therefore, the bubble departure diameter gradually increases. The effect of inlet velocity on bubble departure in the threaded tube is significantly different from that in the smooth tube. In the previous work, it was found that the bubble has a certain axial velocity during the slide process, and further slides and grows until departure under the action of inertial force.

3.4. Heat Transfer Coefficient

In this section, the heat transfer coefficient of the bubble in the threaded tube in subcooled flow boiling is investigated. The simulation work condition is over the range of 200~400 kW/m^2 heat flux, 0.2~0.6 m/s inlet velocity, and 3~20 K subcooling. The heat transfer coefficient is an important index to evaluate heat transfer enhancement. In order to explore the degree of heat transfer enhancement of the threaded tube, the heat transfer coefficients of the threaded tube and the smooth tube are simulated and compared as shown in Figure 12a at different heat flux, 0.4 m/s inlet velocity, and 4 K subcooling. It's observed that the heat transfer coefficient of bubbles in a threaded tube is higher than in a smooth tube, especially at high heat fluxes of 350 and 400 kW/m^2. The calculated heat transfer coefficient in the threaded tube is enhanced by 1.5~12.5%. Obviously, the heat transfer enhancement effect of threaded tubes is not strong from the perspective of the heat transfer coefficient. The main reason is that the heat transfer mode of the bubbles in the threaded tube and the smooth tube is very different. As discussed above, the bubbles in the threaded tube grow and depart at the nucleation site, while the bubbles in the smooth tube depart from the heating wall after sliding. Bubbles will absorb heat in both nucleation and sliding processes before departure in a smooth tube. However, due to the limitation of the thread, the bubble cannot slip in the threaded tube and will only absorb heat during the nucleation process before departure. At the same time, the surface heat fluxes associated with bubble growth in both threaded and smooth tubes are compared as shown in Figure 12b. It can be found that the heat flux carried by bubbles in the threaded tube is much higher than that in the smooth tube. It is speculated that the cavity between adjacent threads can effectively preserve heat and provide a better environment for the growth of heated bubbles due to the special structure of the threaded tube. Therefore, the threaded tube achieves good heat transfer enhancement from the perspective of energy transfer. In addition, it will continue to absorb heat growth when the bubble in the threaded tube has departed, which also shows that the threaded tube enhances heat transfer. It can be seen from Figure 12 that surface heat flux enhancement is much higher than the heat transfer coefficient, which

means temperature difference increase. The special structure of the threaded tube can effectively absorb and preserve heat. The accumulation of heat leads to an increase in the temperature difference between the wall and the bulk cold fluid, which reduces the heat transfer coefficient.

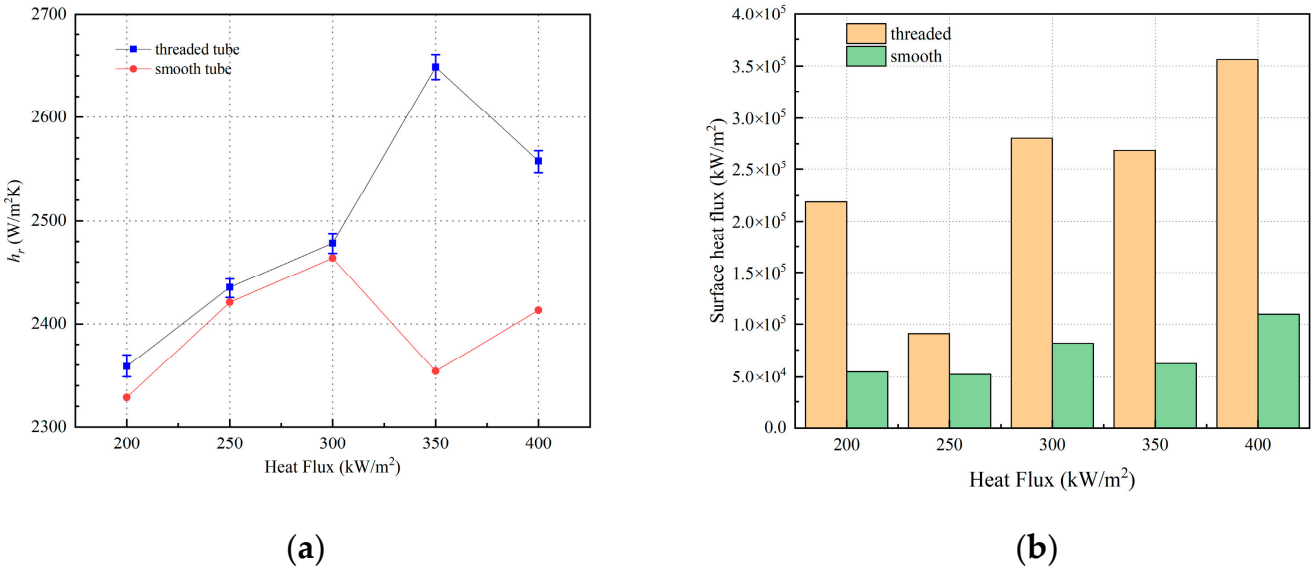

Figure 12. The heat transfer coefficients of the threaded tube and the smooth tube (**a**) and the surface heat fluxes associated with bubble growth in both threaded and smooth tubes (**b**).

Under the determined threaded tube structure, this section also explores the factors affecting the heat transfer coefficient, including heat flux, subcooling, and inlet velocity as illustrated in Figures 13–15. The relationship between bubble departure diameter and heat transfer coefficient is also investigated in this section.

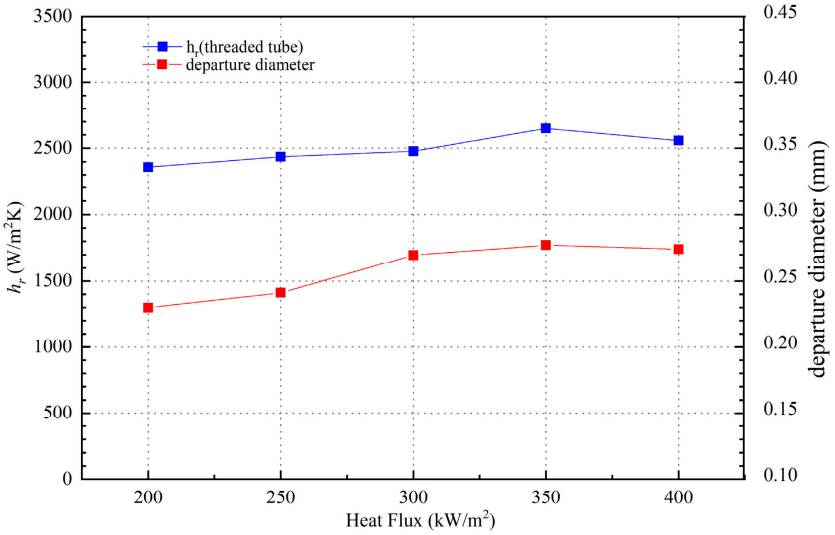

Figure 13. The heat transfer coefficient varies with the heat flux at a condition of 0.4 m/s inlet velocity and 4 K subcooling.

Figure 13 presents the heat transfer coefficient that varies with the heat flux at the condition of 0.4 m/s inlet velocity and 4 K subcooling. The heat transfer coefficient increases with the increase of heat flux. The heat transfer coefficient has the same trend as the bubble departure diameter. It is explained that the formation of a superheated boundary layer under high heat flux conditions makes it easier for bubbles to absorb heat and grow. The heat transfer coefficient increases with the increase of bubble departure diameter. It is

speculated that, on the one hand, the increase in bubble departure diameter indicates that more heat is absorbed before bubble departure, which promotes heat transfer. On the other hand, the increase in bubble departure diameter causes larger bubbles to enter the fluid near the heating wall, which increases the degree of turbulence and promotes heat transfer.

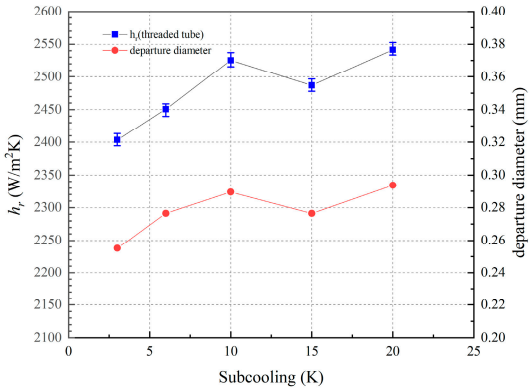

Figure 14. The heat transfer coefficient varies with the subcooling at a condition of 300 kW/m^2 heat flux and 0.4 m/s inlet velocity.

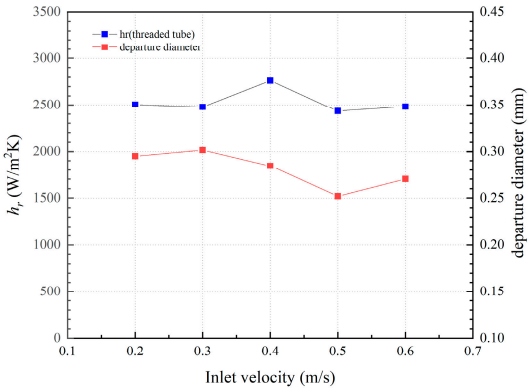

Figure 15. The heat transfer coefficient varies with the inlet velocity at a condition of 300 kW/m^2 heat flux and 4 K subcooling.

Figure 14 exhibits that the heat transfer coefficient varies with the subcooling at the condition of 300 kW/m^2 heat flux and 0.4 m/s inlet velocity. It is seen from Figure 14 that the heat transfer coefficient increases as the subcooling raises. Similarly, the heat transfer coefficient increases with the increase of bubble departure diameter. For the subcooled flow boiling of R134a in the threaded tube, the surface tension plays a role in bubble growth and departure. At higher subcooling, a larger temperature field results in a larger surface tension gradient, which exacerbates the convection between the main stream and the bubble.

Figure 15 shows that the heat transfer coefficient varies with the inlet velocity at the condition of 300 kW/m^2 heat flux and 4 K subcooling. From Figure 15, the maximum heat transfer coefficient is obtained at 0.4 m/s. It is inferred that the inlet velocity of 0.4 m/s provides a good velocity field for bubble growth because a lower inlet velocity slows down the convective cooling of the bubbles, while a higher velocity inhibits the growth of the bubbles and prevents heat from being taken away in time. The velocity field formed by the main fluid in the threaded tube is more consistent with the threaded structure. At this time, the influence of the velocity field on both sides of the thread is more balanced, so that the shape of the bubble is more regular and the heat transfer is promoted. Different from the temperature field, the thread structure has a greater influence on the velocity field. The heat transfer coefficient and the bubble departure diameter no longer have the same trend. The thread increases the degree of turbulence near the heating wall, resulting in a weakening of

the relationship between the heat transfer coefficient and the bubble departure diameter. Analyzing the effects of heat flux, velocity, and subcooling on the heat transfer coefficient, it is found that the heat transfer coefficient depends on the temperature field and velocity field of the bubble.

4. Conclusions

Under the conditions of 200~400 kW/m^2 heat flux, 0.2~0.6 m/s inlet velocity, and 3~20 K subcooling, the bubble behavior in a three-dimensional horizontal threaded tube with a thread tooth height of 0.581 mm was simulated. The effects of inlet velocity, inlet subcooling, and heat flux on bubble departure diameter and heat transfer coefficient were investigated. The following conclusions were obtained:

(1) Under the conditions of 300 kW/m^2 heat flux, 0.4 m/s inlet velocity, and 4 K subcooling, the bubble nucleation was observed in each cavity, and the entire growth process of five kinds of bubbles was recorded. Bubble B2 was collapsed by cold liquid after leaving the heating wall. The bubble growth in the cavity showed certain characteristics. Five kinds of bubbles grew along the radial direction. Unlike bubble B2, the other bubbles did not collapse after departure but grew along the axial direction. The bubble growth in the threaded tube was different from that in the smooth tube. There was no bubble sliding during the bubble growth. Finally, the phenomenon of bubbles passing through the cavity was found, and the coalescence and breakup of bubbles occurred after passing through the cavity.

(2) Under the conditions of 200~400 kW/m^2 heat flux, 0.2~0.6 m/s inlet velocity, and 3~20 K inlet subcooling, the diameter of bubble departure in the threaded tube was between 0.2~0.4 mm. Due to the limitation of the thread, bubbles cannot slide, and the diameter of bubble departure in a threaded tube was generally smaller than that in a smooth tube, but the threaded tube enabled bubbles to achieve secondary growth and departure, thus enhancing heat transfer. When the tooth height was 0.581 mm, the bubble departure diameter increased with the increase of heat flux from 200~400 kW/m^2 and inlet subcooling from 3~20 K and decreased with the increase of inlet velocity from 0.2~0.6 m/s. The main reason is that the heat flux of the bubble provides a superheated environment for the bubble so that the bubble can expand around; When the inlet subcooling increases, the Marangoni effect is enhanced, which increases the sufficient heat flux provided by the heating wall, leading to the increase of bubble departure diameter. Under the condition of high inlet velocity, the shear force acting on the bubble increases, which promotes the departure of the bubble.

(3) Under the conditions of 200~400 kW/m^2 heat flux, the heat transfer coefficient of the bubbles in the threaded tube was higher than that in the smooth tube, especially at a high heat flux of 350 and 400 kW/m^2. The heat transfer coefficient in the threaded tube was increased by 1.5~12.5%. The heat transfer coefficient increased with the increase of heat flux. This is because the superheated boundary layer was formed under the condition of high heat flux, which made it easier for bubbles to absorb heat and grow up. The heat transfer coefficient increased with the increase of the subcooling. The main reason is that the larger temperature field leads to a larger surface tension gradient at the higher subcooling, which aggravates the convection between the main stream and the bubbles. When other conditions remain unchanged, the heat transfer coefficient reached the maximum at 0.4 m/s under the condition of 0.2~0.6 m/s. The inlet velocity of 0.4 m/s provided a good velocity field for bubble growth, because the lower inlet velocity slowed down the convective cooling of bubbles, while the higher velocity inhibited the growth of bubbles.

(4) The heat transfer coefficient and bubble departure diameter had the same change trend under the conditions of 200~400 kW/m^2 heat flux and 3~20 K inlet subcooling. It was concluded that the bubble departure diameter affected the heat transfer coefficient. The heat transfer coefficient can be increased by increasing the bubble departure diameter to enhance the heat transfer. Under different inlet velocity conditions, the relationship between the heat transfer coefficient and bubble departure diameter was weak. It can be

speculated that due to the influence of the thread structure, the turbulence near the heating surface was intensified, and the velocity field around the bubble changed greatly, which affected the heat transfer and bubble behavior.

Author Contributions: Conceptualization, K.L. and B.W.; methodology, K.L.; software, K.L.; validation, K.L.; formal analysis, K.L.; investigation, K.L.; resources, J.W. and J.X.; data curation, B.W.; writing—original draft preparation, K.L.; writing—review and editing, K.L. and B.W.; supervision, J.X.; project administration, J.X.; funding acquisition, J.X. All authors have read and agreed to the published version of the manuscript.

Funding: This research was funded by the National Key R&D Program of China, grant number 2019YFD0901604; Science and Technology Innovation Action Plan of the Shanghai Science and Technology Commission, grant number 19DZ1207503; and the Public Service Platform Project of the Shanghai Science and Technology Commission, grant number 20DZ2292200.

Data Availability Statement: Not applicable.

Conflicts of Interest: The authors declare no conflict of interest.

Nomenclature

The following NOMENCLATURE and Greek Symbols are used in this manuscript:

NOMENCLATURE	
a	bubble width [m]
b	bubble height [m]
c_p	mixture specific heat capacity [J/kgK]
D	bubble diameter [m]
F	force per unit volume of fluid [N/m^3]
g	acceleration of gravity [m/s^2]
h	latent heat [J/kg]
h_r	heat transfer coefficient
k	turbulent kinetic energy [m^2/s^2]
M	mass source [kg/(m^{3}s)]
p	pressure of interface [N/m^2]
q	heat flux [W/m^2]
S_E	energy source term [W/m^3]
T	mixture temperature [K]
T_f	fluid temperature [K]
T_m	heating wall temperature [K]
t	time [s]
$\vec{u}$	velocity [m/s]
u_τ	shear velocity [m/s]

Greek Symbols	
α	volume fraction
η	mass transfer coefficient [s^{-1}]
λ	mixture conductivity [W/mK]
μ	dynamic viscosity [Ns/m^2]
ν	kinematic viscosity [m^2/s]
ρ	density [kg/m^3]
σ	coefficient of surface tension [N/m]
ϕ	symbolic distance function
ω	turbulent vortex frequency

The following subscripts are used in this manuscript:

Subscripts	
ave	average
eff	effective
l	liquid
lv	liquid to vapor
level	level set
sat	saturation
t	turbulent
v	vapor
vl	vapor to liquid
vol	volume

References

1. Celen, A.; Çebi, A.; Dalkılıç, A.S. Investigation of boiling heat transfer characteristics of R134a flowing in smooth and microfin tubes. *Int. Commun. Heat Mass Transf.* **2018**, *93*, 21–33. [CrossRef]
2. Yang, C.-M.; Hrnjak, P. Effect of helical micro-fins on two-phase flow behavior of R410A evaporating in horizontal round tubes obtained through visualization. *Int. J. Heat Mass Transf.* **2019**, *144*. [CrossRef]
3. Yarmohammadi, S.; Mohammadzadeh, K.; Farhadi, M.; Hajimiri, H.; Modir, A. Multi-objective optimization of thermal and flow characteristics of R-404A evaporation through corrugated tubes. *J. Energy Storage* **2020**, *27*, 101137. [CrossRef]
4. He, G.; Zhou, S.; Li, D.; Cai, D.; Zou, S. Experimental study on the flow boiling heat transfer characteristics of R32 in horizontal tubes. *Int. J. Heat Mass Transf.* **2018**, *125*, 943–958. [CrossRef]
5. Vlasie, C.; Macchi, H.; Guilpart, J.; Agostini, B. Flow boiling in small diameter channels. *Int. J. Refrig.* **2004**, *27*, 191–201. [CrossRef]
6. Ebadian, M.A.; Lin, C.X. A Review of High-Heat-Flux Heat Removal Technologies. *J. Heat Transf.* **2011**, *133*, 110801. [CrossRef]
7. Meena, C.S.; Kumar, A.; Roy, S.; Cannavale, A.; Ghosh, A. Review on Boiling Heat Transfer Enhancement Techniques. *Energies* **2022**, *15*, 5759. [CrossRef]
8. Cao, Y.; Kawara, Z.; Yokomine, T.; Kunugi, T. Visualization study on bubble dynamical behavior in subcooled flow boiling under various subcooling degree and flowrates. *Int. J. Heat Mass Transf.* **2015**, *93*, 839–852. [CrossRef]
9. Pipathattakul, M.; Mahian, O.; Dalkilic, A.S.; Wongwises, S. Effects of the gap size on the flow pattern maps in a mini-gap annular channel. *Exp. Therm. Fluid Sci.* **2014**, *57*, 420–424. [CrossRef]
10. Yan, J.; Xie, J. Comparative Proteome Analysis of Shewanella putrefaciens WS13 Mature Biofilm Under Cold Stress. *Front. Microbiol.* **2020**, *11*, 1225. [CrossRef]
11. Kang, Z.; Jiang, S.; Hong, Y.; Fan, J. Squid-like soft heat pipe for multiple heat transport. *Droplet* **2022**, *1*, 182–191. [CrossRef]
12. Kang, Z.; Hong, Y.; Jiang, S.; Fan, J. Composite filament with super high effective thermal conductivity. *Mater. Today Phys.* **2023**, *34*, 101067. [CrossRef]
13. Zhang, P.; Fu, X.; Wang, R.Z. Flow Boiling Patterns of Liquid Nitrogen in Micro-Tubes. In Proceedings of the ASME 2008 Heat Transfer Summer Conference collocated with the Fluids Engineering, Energy Sustainability, and 3rd Energy Nanotechnology Conferences, Jacksonville, FL, USA, 10–14 August 2008; pp. 741–745. [CrossRef]
14. Wu, Z.; Sundén, B. Heat transfer correlations for elongated bubbly flow in flow boiling micro/minichannels. *Heat Transf. Eng.* **2016**, *37*, 985–993. [CrossRef]
15. Mohanty, R.L.; Das, M.K. A critical review on bubble dynamics parameters influencing boiling heat transfer. *Renew. Sustain. Energy Rev.* **2017**, *78*, 466–494. [CrossRef]
16. Du, J.; Zhao, C.; Bo, H.; Ren, X. The Modeling of Bubble Lift-Off Diameter in Vertical Subcooled Boiling Flow. *Energies* **2022**, *15*, 6857. [CrossRef]
17. Yu, S.; Peng, C.; Zhang, Z.; Cheng, N. Experimental investigation and model prediction of sliding bubble dynamics in vertical subcooled boiling flow. *Int. J. Heat Mass Transf.* **2023**, *200*, 123520. [CrossRef]
18. Yang, L.X.; Guo, A.; Liu, D. Experimental Investigation of Subcooled Vertical Upward Flow Boiling in a Narrow Rectangular Channel. *Exp. Heat Transf.* **2014**, *29*, 221–243. [CrossRef]
19. Ali, R.; Palm, B.; Maqbool, M.H. Flow boiling heat transfer of refrigerants R134A and R245fA in a horizontal micro-channel. *Exp. Heat Transf.* **2012**, *25*, 181–196. [CrossRef]
20. Alam, T.; Li, W.; Yang, F.; Chang, W.; Li, J.; Wang, Z.; Khan, J.; Li, C. Force analysis and bubble dynamics during flow boiling in silicon nanowire microchannels. *Int. J. Heat Mass Transf.* **2016**, *101*, 915–926. [CrossRef]
21. Matin, M.; Fazeli, A.; Moghaddam, S. Physics of transition to annular flow in microchannel flow boiling process. In Proceedings of the 2018 17th IEEE Intersociety Conference on Thermal and Thermomechanical Phenomena in Electronic Systems (ITherm), Piscataway, NJ, USA, 29 May–1 June 2018; IEEE: Piscataway Township, NJ, USA, 2018.
22. Abdul-Majeed, B.A.; Jawad, H.R. Analysis of Shell and Double Concentric Tube Heat Exchanger Using CFD Application. *J. Eng.* **2019**, *25*, 21–36. [CrossRef]
23. Marín, P.; Ordóñez, S.; Díez, F.V. Rational design of heating elements using CFD: Application to a bench-scale adiabatic reactor. *Comput. Chem. Eng.* **2011**, *35*, 2326–2333. [CrossRef]
24. Guo, L.; Zhang, S.; Chen, Y.; Cheng, L. Research of Flow Boiling Bubble Dynamics in Vertical Rectangular Minichannel. In Proceedings of the 2010 Asia-Pacific Conference on Power Electronics and Design, Wuhan, China, 30–31 May 2010; pp. 16–19. [CrossRef]
25. Ling, K.; Son, G.; Sun, D.-L.; Tao, W.-Q. Three dimensional numerical simulation on bubble growth and merger in microchannel boiling flow. *Int. J. Therm. Sci.* **2015**, *98*, 135–147. [CrossRef]
26. Xu, Y.; Zhu, Z.; Xiong, X. Numerical study of flow boiling flow patterns and pressure drop of R134a in small tubes under high flight acceleration. *J. Braz. Soc. Mech. Sci. Eng.* **2020**, *42*, 1–10. [CrossRef]
27. Zhuan, R.; Wang, W. Simulation of subcooled flow boiling in a micro-channel. *Int. J. Refrig.* **2011**, *34*, 781–795. [CrossRef]
28. Kang, Z.; Shou, D.; Fan, J. Numerical study of single-loop pulsating heat pipe with porous wicking layer. *Int. J. Therm. Sci.* **2022**, *179*, 107614. [CrossRef]
29. Lee, W.; Son, G.; Yoon, H.Y. Numerical study of bubble growth and boiling heat transfer on a microfinned surface. *Int. Commun. Heat Mass Transf.* **2012**, *39*, 52–57. [CrossRef]

30. Kang, Z.; Shou, D.; Fan, J. Numerical study of a novel Single-loop pulsating heat pipe with separating walls within the flow channel. *Appl. Therm. Eng.* **2021**, *196*, 117246. [CrossRef]
31. Ma, H.; Cai, W.; Chen, J.; Yao, Y.; Jiang, Y. Numerical investigation on saturated boiling and heat transfer correlations in a vertical rectangular minichannel. *Int. J. Therm. Sci.* **2016**, *102*, 285–299. [CrossRef]
32. Wang, J.; Wang, B.; Xie, J.; Lei, K.; Yu, B.; Sun, Y. Numerical Simulation Research of Bubble Characteristics and Bubble Departure Diameter in Subcooled Flow Boiling. *Mathematics* **2022**, *10*, 4103. [CrossRef]
33. Lee, W.H. A pressure iteration scheme for two-phase flow modeling. In *Computational Methods for Two-Phase Flow and Particle Transport*; World Scientific Publishing: Singapore, 2013; pp. 61–82.
34. Issa, R. Solution of the implicitly discretised fluid flow equations by operator-splitting. *J. Comput. Phys.* **1986**, *62*, 40–65. [CrossRef]
35. Chen, C.; Li, K.; Lin, T.; Li, W.-K.; Yan, W.-M. Study on heat transfer and bubble behavior inside horizontal annuli: Experimental comparison of R-134a, R–407C, and R-410A subcooled flow boiling. *Case Stud. Therm. Eng.* **2021**, *24*, 100875. [CrossRef]
36. Owoeye, E.J. Bubble transport in subcooled flow boiling. *Nucl. Eng. Des.* **2015**, *289*, 126–143. [CrossRef]
37. Fu, X.; Zhang, P.; Huang, C.; Wang, R. Bubble growth, departure and the following flow pattern evolution during flow boiling in a mini-tube. *Int. J. Heat Mass Transf.* **2010**, *53*, 4819–4831. [CrossRef]
38. Han, C.-Y.; Griffith, P. The mechanism of heat transfer in nucleate pool boiling—Part I: Bubble initiaton, growth and departure. *Int. J. Heat Mass Transf.* **1965**, *8*, 887–904.
39. Sugrue, R.; Buongiorno, J. A modified force-balance model for prediction of bubble departure diameter in subcooled flow boiling. *Nucl. Eng. Des.* **2016**, *305*, 717–722. [CrossRef]